International Journal of Electronics and Applied Research (IJEAR) **vol. 4, issue 1, July 2017**
Online (*http://eses.net.in/ESES Journal)* ISSN 2395-0064

Synthesis of Schumann resonance background signal in time domain

Kudintseva I.G.[1], Nikolayenko S.A.[1], Nickolaenko A.P.[2], Hayakawa M.[3]
[1] *V.N. Karazin Kharkov National University*
4 Svoboda square, 61077 Kharkov, Ukraine
[2] *A.Ya. Usikov Institute for Radio-Physics and Electronics, National Academy of Sciences of Ukraine*
12 Academician Proskura Street, 61085 Kharkov, Ukraine
E-mail: sasha@ire.kharkov.ua
[3] *Hayakawa Institute of Seismo Electromagnetics, Co. Ltd., UEC Incubation Center-508,*
1-5-1 Chofugaoka, Chofu Tokyo, 182-8585, Japan
E-mail: hayakawa@hi-seismo-em.jp

Abstract

Simulation of global electromagnetic resonance signal is of great importance for both the theory and measurement practice. We describe the simulation and present the main properties of artificial Schumann resonance signals. We show that synthesized records explain many features observed experimentally. The artificial signal is a succession of random pulses, and each of them was found from the solution of Schumann resonance problem in the time domain. To obtain the model signal, random variables were used having exponential (mutual time delay of pulses), normal (random amplitudes of lightning strokes), and uniform (accidental source–observer distances) distributions. The particular model treats only the vertical electric field component. It is proposed to use such signals for simulating the natural noise and for calibrating the receiving equipment.

1. Introduction

Global electromagnetic resonance takes place in the spherical cavity formed by the ground and ionosphere. It was predicted by Schumann in 1952 [Schumann, 1952] and is often regarded as Schumann resonance (SR). The phenomenon is observed in the extremely low frequency (ELF) band (3 – 3000 Hz), the electromagnetic oscillations are driven by radiation of lightning strokes, and resonances are observed as peaks in the power spectra of natural radio noise at frequencies 8, 14, 20 Hz, etc. Description of SR, its properties and applications together with vast literature might be found in the books by Nickolaenko and Hayakawa [2002, 2014].

Synthesis of artificial electromagnetic noise in the Earth–ionosphere cavity and studying its properties is interesting in two ways. Firstly, such a signal allows us to inspect the consistency of common explanations of experimentally observed features pertinent to SR signals. On the other hand, a realistic digitally generated artificial signal might be converted into the analog form and used as a standard testing signal for calibration of the low frequency receivers exploited at different observation sites.

2. Signal model

According to the modern concept, natural radio noise at ELF is formed by a random sequence of pulses arriving from global thunderstorm activity. Radiation from the most distant lightning strokes can reach an observer owing to the low losses in the thin dielectric gap between the Earth and ionosphere. These pulses compose the natural ELF radio signal, which might be described as the following random succession in the time domain (Nickolaenko, 1997; Nickolaenko and Hayakawa, 2002, 2014):

$$E(t) = \sum_{k=-\infty}^{\infty} A_k \cdot e_k(t - t_k) \tag{1}$$

$$H_X(t) = H_{EW} = \sum_{k=-\infty}^{\infty} A_k \cdot h_k(t - t_k) \cdot [-\cos(B_k)] \tag{2}$$

$$H_Y(t) = H_{NS} = \sum_{k=-\infty}^{\infty} A_k \cdot h_k(t - t_k) \cdot \sin(B_k) \tag{3}$$

Here t is the current time, A_k is the random amplitude of the k-th pulse, t_k is its arrival time, B_k is the azimuth of the lightning stroke that has emitted this pulse, which depend on the random source–observer distance D_k. The quantities A_k, t_k, D_k and B_k are random and mutually independent variables. Functions $e_k(t)$ and $h_k(t)$ are correspondingly the waveforms of electric and magnetic field components of the k-th pulse

$$e(t) = E_A \cdot \mathrm{Re}\left\{ A_\nu \cdot \tau^{-B_\nu} \left[Q_{-1} + (Q_0 - 1)B_\nu + \left(\frac{Q_1}{\tau} - 1 \right) B_\nu (B_\nu + 1) + B_\nu (B_\nu + 1)^2 \sum_{n=1}^{\infty} \frac{\tau^n P_n(x)}{(n - B_\nu)(n+1)} \right] \right\} \tag{4}$$

$$h(t) = H_A \cdot \mathrm{Im}\left\{ \frac{\tau^{(1-B_\nu)} \sqrt{1 - x^2}}{\sqrt{(1 - 2x\tau + \tau^2)^3}} \right\}, \tag{5}$$

where $E_A = M_C/(2\pi \cdot ha^2 \cdot \varepsilon_0)$ and $H_A = M_C/(2\pi \cdot ahc^2)$ (h ionospheric height, a Earth's radius, c light velocity and ε_0 dielectric constant of free space) are amplitudes of the electric and magnetic fields that depend on the magnitude of the current moment of the source M_C. We assume for the simplicity that $E_A = H_A = 1$; $\tau = \exp(it/A_\nu)$ (A_ν will be given later) is the time factor, $x = \cos(\pi D/20)$ is the source–observer distance D measured in megameters (1 Mm = 1000 km). Functions $Q_{-1} = (1 - x\tau) / (1 - 2x\tau + \tau^2)^{3/2}$ and $Q_1 = \ln\{[\tau - x + (1 - 2x\tau + \tau^2)^{1/2}] / (1 - x)]\}$ were obtained from the generating function of the Legendre polynomials $Q_0 = (1 - 2x\tau + \tau^2)^{-1/2}$ by using its integration or differentiation in respect with the parameter τ. Analytical solutions (4) and (5) are based on the linear frequency dependence of the propagation constant of ELF radio wave of the form $\nu(\omega) = A_\nu \omega + B_\nu$ with the parameters found from observational data, and $A_\nu = (1/6 - i/100)/(2.\pi)$ and $B_\nu = -1/3$[see Nickolaenko and Hayakawa ,1998, 2002, 2014; Nickolaenko, 1997; Nickolaenko et al., 1999, 2004a, b; Myand et al., 2001; Nickolaenko and Rabinowicz, 2001].

Synthesis of the background radio noise at ELF exploits the formal solution of the SR problem in the time domain discussed in detail in the works by Nickolaenko and Hayakawa,1998, 2002, 2014, Nickolaenko,1997, Nickolaenko et al., 1999, 2004a, b; Myand et al., 2001; Nickolaenko and Rabinowicz, 2001. Formal summation in equations (1)–(3) is carried out in the infinite limits. However, in accordance with the causality principle, the pulse amplitude turns to zero when the time argument is negative: $t - t_k < 0$.

The amplitudes of waveforms $e_k(t)$ and $h_k(t)$ decreases with time, so that one can put them equal to zero when the condition is held $t - t_k > t_p$. We will use the time interval $t_p = 0.3$ s, so that only those impulses participate in the summation that arrive the observer from 0 to 0.3 seconds prior to the current time t. A radio pulse circles the globe approximately three times during 0.3 s, and simultaneously; its amplitude significantly decreases due to the wave attenuation and dispersion. It is assumed, as usual, that the lightning strokes occur independently, so that the arriving pulses form a Poisson succession with the rate of λ events per second, while the relative lag in time has the exponential distribution [Nickolaenko, 1981].

Formulas (4) and (5) describe a pulse propagating in the closed spherical Earth–ionosphere cavity, which repeatedly circles the globe and accounts for the phenomenon of global electromagnetic resonance. Only the vertical electric field is treated in what follows. The horizontal magnetic field might be modeled similarly, but the model source azimuth should be introduced as an additional random variable.

We assume that the random source–observer distance is uniformly distributed in a certain interval that the pulsed amplitudes obey the normal (Gauss) distribution, and the mutual arrival time delay of adjacent pulses is described by an exponential distribution. Thus, the three random variables must be used in simulations having the uniform, the Gauss, and the exponential distribution.

The source–observer distance is generated with the help of standard FORTRAN procedure ran1(idum). Here, the initial value of random succession is equal to idum = e·π = 8.53974322674, and it triggers the pseudo-random number generator. The obtained values r_k are uniformly distributed in the open interval (0, 1). We transform r_k into the distances D_k from the 7 – 12 Mm segment by using the following relation $D_k = D_A + r_k \cdot \Delta D$, where the "initial" value D_A = 7 Mm, and the interval of distance fluctuations ΔD = 5 Mm. The pulse delay was calculated by using the expdev (idum1) procedure, where the initial value was idum1 = π/e = 1,15572734979. The pseudo-random variable ζ_k thus obtained has the exponential distribution and provides the mutual time lag of pulses equal to $\tau_k = \zeta_k / \lambda$. We suggest that the amplitude of radio pulses produced by lightning strokes has the normal (Gauss) distribution. It is generated by the standard sub-routine gasdev (idum2) with the initial value of the pseudo-random sequence idum2 = e·e = 7.38905609893. The random variable g_k thus obtained was converted into the pulsed amplitude A_k by using the following relation: $A_k = g_k \cdot \sigma_A + A_{AV}$ where the average amplitude and its variance are equal to A_{AV} = 1 and σ_A = 2.6666 correspondingly. The arbitrary units of amplitude are proportional to the average current of 15 kA and its standard deviation of 40 kA [Nickolaenko, 1981; Nickolaenko and Hayakawa, 2002, 2014].

Generators of the random numbers have yielded three successions relevant to the source–observer distance, to the pulsed amplitude and to the mutual delay of pulses. The full sequences contained $5.5 \cdot 10^5$ numbers. To demonstrate the compliance of these variables with the imposed requirements, we show the histograms of 'experimental' distributions of all these variables in Figure 1. The interval of alterations of particular random variable was divided into 60 sub-intervals, and we counted the number of events when the random number falls into the particular fragment. The corresponding histograms y = W(x) are shown in Figure 1.

The top histogram (Figure 1a) depicts the density distribution of the D_k source–observer distance. The horizontal axis shows the distance in the range from 0 to 20 Mm. The ordinate shows the number of

events when the random distance D_k was found within each of the 60 intervals. It is evident that casual distances to the field source were uniformly distributed in the area ranging from 7 to 12 mm.

The plot in Figure 1b demonstrates the histogram of the pulsed amplitudes. Here, the horizontal axis depicts the amplitude in arbitrary units divided into 60 sub-intervals, and the vertical axis shows (on the logarithm scale) the number of events when the random variable is found in the corresponding interval. The normal (Gauss) distribution is represented by a parabola in such a coordinate system as we observe in Figure 1b. The dots in the plot depict the postulated Gaussian curve with $A_{AV} = 1$ and $\sigma_A = 2.6666$. It is worth noting here that we apply the normal distribution for the pulsed amplitudes of the source currents, which is unusual since the amplitude might become negative. Such a distribution is rather convenient in the computations, besides it corresponds to observations [Nickolaenko, 1981; Nickolaenko and Hayakawa, 2002, 2014] and allows us simultaneously to consistently describe both the prevailing "negative" lightning strokes that transfer the negative charge from a cloud to the land and the “positive” strokes carrying the positive charge. The more detailed description and justification of the normal amplitude distribution might be found in Nickolaenko [1981].

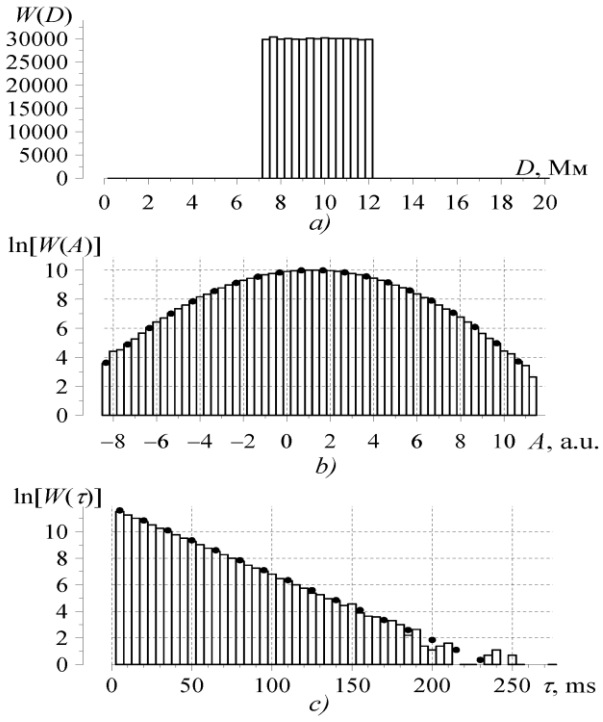

Figure 1: Histograms and distribution functions of random variables used in the model SR signal.

The plot in Figure 1c shows the density distribution function of the mutual pulse delay. The abscissa here represents the time delay in ms, and the number of events falling within the selected interval is shown along the vertical axis on the logarithm scale. Dots denote the postulated distributions having the flux density of λ= 50 pulses per second. As might be seen from Figure 1, we use successions of quasi-random numbers really satisfying the specified probability distributions.

3. Random time series

Time realization of SR signal was computed by using equations (1)-(5) with the help of the quasi-random variables mentioned above. To eliminate the "edge effect", which is associated with the beginning of random numbers, the first 1024 values were discarded from the succession. To completely avoid any transient process in the created synthetic time realization, we further discarded the first 5 seconds of the record when performing spectral processing.

Since the ensembles of random variables are fixed, the synthetic time realizations acquired a kind of "reproducibility" in regard to changes of the pulse rate. Such a feature is out of reach in the natural signals. We present in Figur e 2 two 60 s records relevant to the flux density λ = 1 (upper panel) and λ = 50 pulses per second (lower panel). The current observation time t was quantified with the sampling frequency of 204.8 Hz, so that 2048 points of the records occupy the time interval of 10 s.

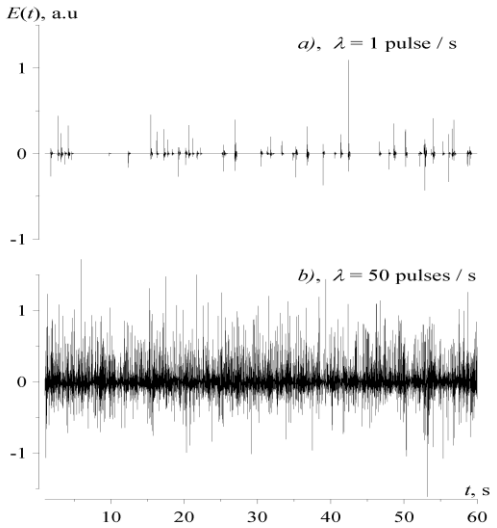

Figure 2: One-minute fragments of artificial SR signal for λ = 1 and λ = 50 pulses per second.

The abscissa of Figure 2 shows the time from 1 to 60 seconds, and the synthesized radio noise E(t) is shown on the vertical axes in arbitrary units for the flux density $\lambda = 1$ (upper panel) and $\lambda = 50$ pulses/second (lower panel). Obviously, the artificial noise signal deviates from the habitual experimental records in two aspects.

The first one is that onsets of individual pulses are very short and sharp. This feature is especially clear in the upper plot where the flux density is so low that individual pulses are easily resolved in the record. The pulse rate is increased by the factor of 50 in the lower panel. Physically, this means that the arrival times were "compressed" by this factor, while the temporal characteristic of individual pulses remained the same. As a result, the pulses of the upper plot occupying 60 s interval were "shifted like beads of a necklace" leftward to occupy 1.2 s time interval at the lower frame, so that their waveforms severely overlap and cannot be resolved in the time record, except, maybe, pulse tops.

The second aspect is that no ELF transients or Q-bursts are visible arriving from the powerful lightning strokes.

Both these distinctive features are conditioned by the particular model, in which we do not take into account the frequency response of a typical SR receiver together with the relatively rare Q-bursts (these occur at a rate of one event in a few minutes). The typical radio receiver for the SR observations has a bandwidth of 4–40 Hz, and it considerably smoothes the fast excursions in the pulsed waveforms. If one sends the synthesized signal through the digital-to-analog converter and feeds it afterwards to the input of a receiver, the output realization will be similar to the records of natural ELF background radio noise.

One may observe that the positive deviations from zero prevail in the time realization E(t) over the negative excursions (see Figure 2b). This is due to dominance of the negative lightning strokes that provide the positive onsets in the observed pulsed electric field. This feature might be expected in accordance with the amplitude distribution postulated. As one may see, the flux of 50 impulses per second is rather dense, so that individual pulsed waveforms substantially overlap in the record. The time realization itself does not show to what an extent the artificial signal is similar to observations. The ELF spectra are much more informative in this sense, and we turn to them now.

4. Amplitude spectrum of model data

After creating the time domain realization of SR signal, we can compute its spectrum by using fast Fourier transform (FFT). When doing this, we will ignore, similarly to the newcomers to the SR investigations, both the noisy nature of the time domain record and the basic features of Fourier transform. We take a long enough fragment of the time realization (about 40 minutes long) and compute its Fourier transform. The amplitude spectrum thus obtained is depicted in Figure 3. The signal frequency covering the SR band is plotted on the abscissa, and the spectral amplitude is shown on the ordinate in arbitrary units on logarithmic scale.

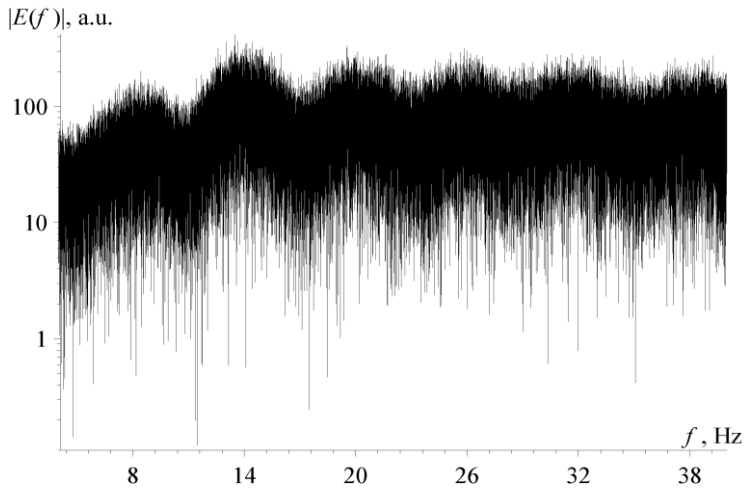

Figure 3: Amplitude spectrum of synthetic radio signal for λ = 50 pulses/s when the processed time domain realization is ~40 minutes long.

One may observe that a Fourier-transform of a temporal realization of noise turns into a noise in the frequency domain regardless the length of the original time realization. The reason is that an increase in the record duration T does not trigger the data averaging. Instead, it increases the frequency resolution in the spectrum $\Delta f = 1/T$, so that the distance is reduced between the separate points on the frequency axis. As might be seen from Figure 3, SR is clearly visible in the random spectrum. Similar spectra usually puzzle the experimenters that joined the SR community and just started their measurements. For obtaining the

customary power (or amplitude) spectrum, one has to apply some averaging of data that stabilizes the spectral estimates.

This might be performed in two possible ways. The first one is based on the moving average of the spectral estimates. Such a procedure improves spectra due to the fact that fluctuations at different frequencies are mutually independent. Therefore, averaging over frequencies (spectral smoothing) reduces noise and becomes equivalent to averaging over the ensemble of independent realizations.

The second technique of data smoothing data divides the initial time record into pieces of short standard length with further calculation of the power spectra relevant to each of these segments. Averaging of individual power spectra over the ensemble of segments provides a smooth average spectrum, and thus the stable average power spectrum is obtained. The amplitude spectrum might be computed as the square root of the power spectrum. The standard length of the time realization used in Fourier transform must provide a reasonable frequency resolution. Since SR frequencies are 8, 14, 20 Hz, etc., the resolution of 0.1 Hz is usually selected, so that the standard length of an elementary temporal segment of the record is equal to 10 seconds.

5. Dynamic spectra (sonograms)

Dynamic spectra or the sonograms of SR present alterations in the power or amplitude spectra over the time–frequency plane. Such 2D plots clearly illustrating the signal properties are shown in Figure 4 for the three fixed flux densities of atmospherics λ = 1, 10, and 110 pulses per second (from top to bottom). The horizontal axes depict the time in seconds (we use the power spectra of elementary 10 s fragments of the record). The vertical axes show the signal frequency in Hz. The spectral intensity is demonstrated by black inking, and relevant scales are given on the right of each sonogram.

As one may observe, the dark horizontal treks are visible corresponding to the resonance peaks in the dynamic spectra, although the global resonance outline is blemished by the noise present in sonograms. By comparing panels, we note that fluctuations significantly increase when the flux density is low, so it is more difficult to observe the resonance structure in the top panel, especially, in the vicinity of the first resonance mode at 8 Hz.

We must remind that all three records were synthesized by using the same sequences of quasi-random numbers. Simply, in computations shown by the upper map in Figure 4, the pulses are rather rare (see Figure 2), and the model time domain data exploit only the initial section of the full random numbers. The lowest frame depicts a situation when the pulse rate has increased by the factor of 110 in comparison with the upper frame. The horizontal trails of resonance peaks became evident in this panel at least for the first three resonance modes having peak frequencies of 8, 14, and 20 Hz. The middle panel corresponding to λ = 10 pulses/s occupies the intermediate position in this context.

The amount of random numbers used in computations for the lower panel of Figure 4 has significantly increased, but its initial section remains coincident with the sets implied in computations demonstrated by panels for λ = 1 and 10 pulses per second.

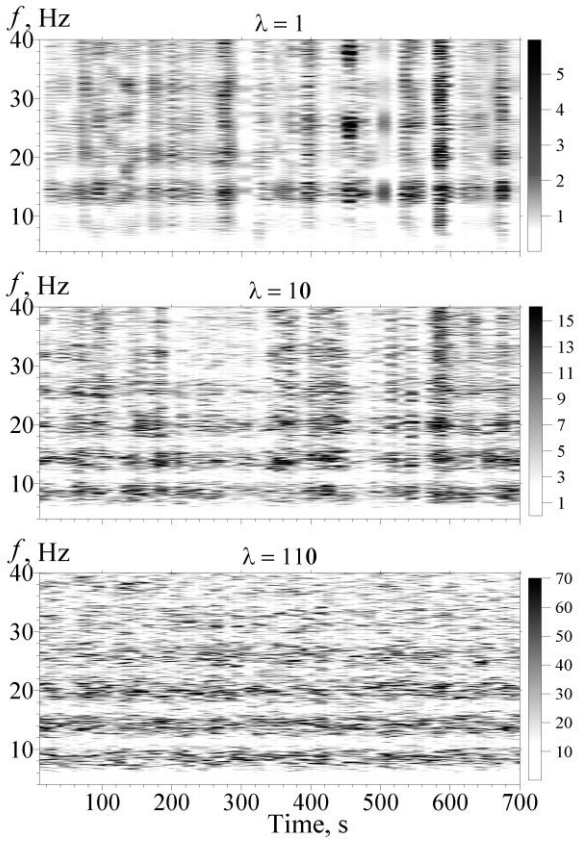

Figure 4: Dynamic spectra for atmospheric fluxes λ = 1, 50, and 110 pulses /s.

Owing to the low flux density of atmospherics on the upper panel of Figure 4, the vertical stripes are clearly visible in sonograms. These appear when the number of pulses arrived in the 10 s elementary time segment is rather small. When this number is reduced to 2 events in the segment which is often the case for $\lambda = 1$, the spectra acquire characteristic interference pattern (see below), so that the dynamic spectrum demonstrates a regular vertical sequence of white and dark horizontal bars. When the flux density is high, the sharp peaks and dips in the power spectrum become smoothed, and the strips become practically absent in the lower dynamic spectrum. Nevertheless, the fine structure is still present in the spectrum, and the sonogram fragmentation is observed along the frequency axis (in vertical direction).

6. Natural stabilization of spectra

We digitized the model time domain record with the sampling frequency of f_s = 204.8 Hz, which is close to the values commonly used in measurements. The segment of standard 10 s duration thus contains 2048 samples. The FFT of such a realization provides the frequency resolution of 0.1 Hz. It is obvious that an elementary spectrum remains a separate piece of noise, but fluctuations subside after averaging (or accumulating) of elementary spectra. The stabilization is improved with an increase of the ensemble of elementary spectra involved in averaging (accumulation). The relevant phenomenon was regarded as natural stabilization of spectral estimates in Nickolaenko and Hayakawa [2002].

We demonstrate in Figure 5 changes of the SR power spectra of the synthesized time domain radio signal for the set of flux densities λ = 1, 10, 50, and 110 events per second. Four panels are shown in this figure computed for increasing the accumulation time. The abscissas indicate the frequency in Hz and the ordinates depict the spectral density in arbitrary units on the logarithmic scale.

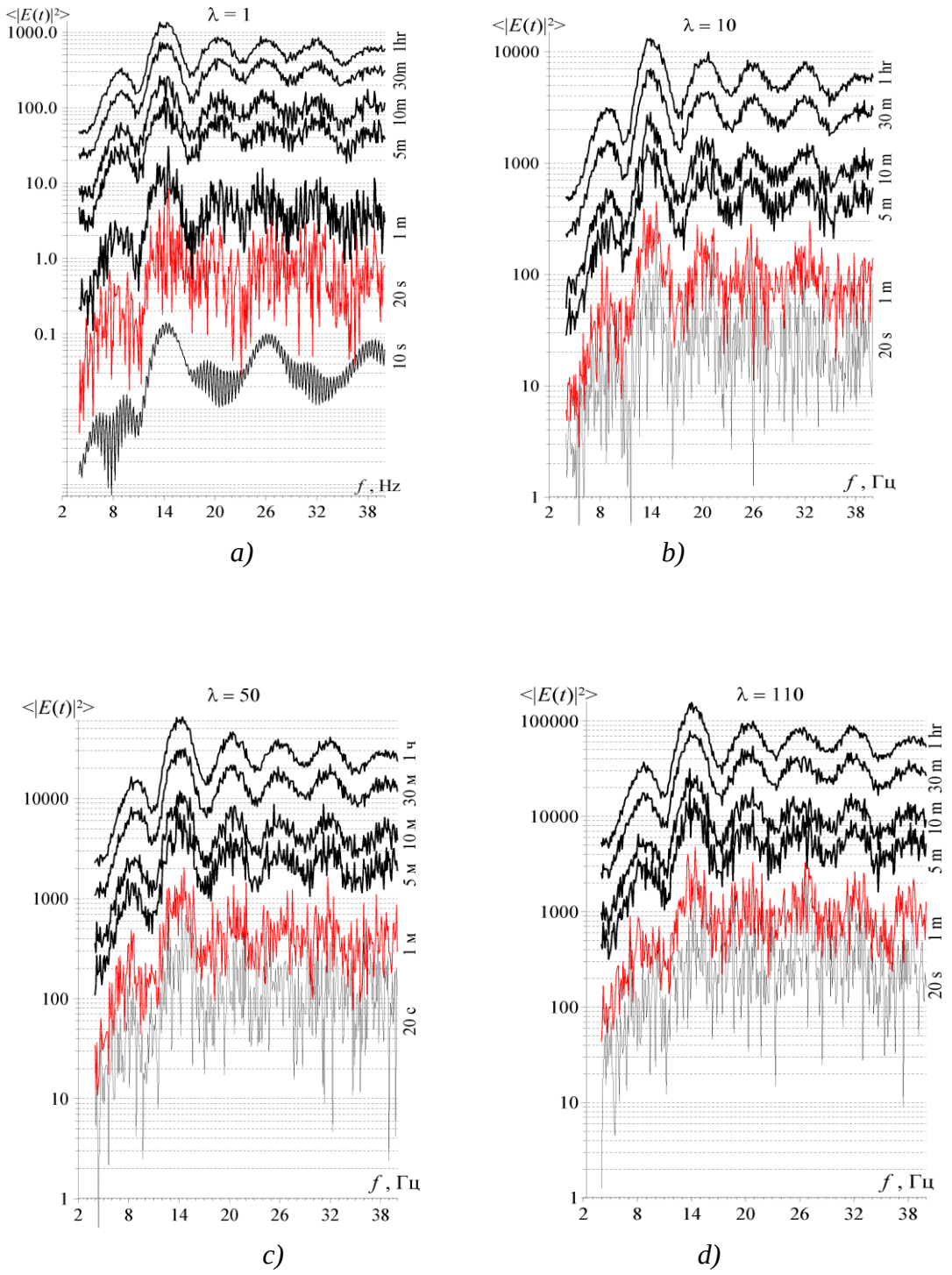

Figure 5: Changes and stabilization of spectra due to accumulation for the atmospheric flux densities of 1 (a), 10 (b), 50 (c) and 110 (d) pulses/s.

Each panel in Figure 5 corresponds to the random radio signal generated with different atmospheric flux densities of λ = 1, 10, 50, and 110 events per second. The top plots in each of the four panels illustrate the power spectra accumulated during 1 hour. These spectra are rather smooth, and all of them have similar patterns because the impact of random factors was substantially reduced by the accumulation. We know that the general resonance pattern is determined by the frequency dependence of propagation constant of ELF radio waves and by distribution of the source–observer distances. We use in this model the uniform distance distribution in a range from 7 to 12 mm, This is why the first resonance peak in the power spectrum of vertical electric field at 8 Hz is lower than the second one lying at 14 Hz.

The lowest lines in each panel in Figure 5 (except for Figure 5a) show the power spectra accumulated during the first 20 seconds of record (the sum of two elementary spectra computed for adjacent time domain segments of 10 s duration each). Corresponding accumulation time of 20 s is shown on the right of the graph. The plots have an irregular form, and resonance peaks are substantially masked by fluctuations arising from the pulse interference.

The more smooth red plots are found above the lowest lines. These were obtained by accumulation of the six elementary power spectra, and the relevant accumulation time of 1 minute is shown to the right of the plots. An increase in accumulation time lifts the resulting power spectrum above the frequency. Concurrently, the regular resonance pattern becomes more pronounced. This occurs because the peaks and the dips of fluctuations in individual spectra do not coincide, and they compensate each other when summing. This process is illustrated by the spectra accumulated during the 1, 5 and 10 minute intervals. Since the resonance peaks become well resolved when the accumulation time reaches 5 or 10 minutes, these accumulation (averaging) intervals are commonly used in the observations. These durations were found empirically from the experimental data.

Plots collected in Figure 5 show that gradual stabilization of the spectral estimates is present everywhere, it occurs approximately similarly in all panels, and the final spectral outline does not significantly depend on the pulse flux.

In case when we increase the accumulation time to 30 minutes or even to 1 hour (the summing involves 180 or 360 elementary spectra), the fine structure in the spectral pattern will be greatly reduced. However, it will not disappear completely. Applying the accumulation time exceeding 1 hour is unreasonable, since the conditions of quasi-stationary statistical process are violated: the global thunderstorms drift around

the planet during the day. As a result, distribution of the source–observer distances varies on the diurnal scale, and the resonance pattern slowly varies with time [Nickolaenko and Hayakawa, 2002, 2014].

Plots in Figure 5 demonstrate a very important feature of SR signals: a considerable accumulation time is necessary for obtaining the stable spectral estimates. Indeed, if we assume that the flux density is λ = 50 pulses/s, about 1000 pulses will arrive an observer during 20 s, and this number seems to be quite sufficient for obtaining stabile results. However, the relative fluctuations in the power spectra obviously exceed the customary estimate of the central limit theorem: $1000^{-½}$ ≈3%. Measurements and model computations indicate that the level of 3% fluctuations is reached when the accumulation time is about some tens of minutes. The corresponding number of independent pulses arrived an observer reaches several tens – hundreds of thousands! Such a slow stabilization of SR spectra is pertinent both to observations and to our model. It is explained by genuine nature of terrestrial radio noise. During the elementary observation time of 10 s, the interference will inevitably arise in the spectrum between individual pulses arriving from different lightning strokes at different times. This interference pattern will finally disappear when the averaging time goes to infinity provided that the random process is of the Poisson type [see, e.g. Tikhonov, 1982]. However, the interference reduction goes much slower due to fluctuations in the pulse arrival times than stabilization in a normal (Gauss) random process, to which the central limit theorem is valid. The great accumulation times arise from the Poisson nature of the process.

The second factor explaining the slow spectral stabilization is conditioned by the energy losses in the Earth–ionosphere cavity. Amplitude of individual pulses decreases in time due to wave attenuation and dispersion. Therefore, averaging procedure incorporates a limited number of lightning strokes. This number is determined by the rate of temporal decrease of the pulsed amplitude, so that even infinite accumulation (averaging) period includes a truncated quantity of pulses. This is why interference cannot disappear completely even during the long-term accumulation: the cavity itself “trims” the ensemble of events.

Plots in Figure 5 demonstrate natural stabilization of spectral estimates during accumulation, which is similar to the observations that were shown in Figure 4.32 of the book by Nickolaenko and Hayakawa [2002]. It was noted that the model for λ = 100 pulses per second is in accord with the experimental data on the natural SR spectra. The present treatment implies the pulse rates covering two orders of magnitude, and additionally the duration of synthetic record was increased up to more than 60 minutes.

7. Interference of two pulses and observed spectral outline

We showed that any interference in spectra reduces with accumulation time. To demonstrate a specific case we included an additional spectrum in Figure 6a for $\lambda = 1$. This is the lowest plot showing the power spectrum of the first 10 s fragment of the time realization. One may observe the characteristic "beating" arising from the two-pulse interference.

It is known that the mean and the RMS (root mean square) values of the random mutual pulse delay are equal to each other in the Poisson succession. Therefore, the number of pulses in a standard time interval fluctuates severely. It is quite possible that a time interval of 10 s duration contains only a couple of pulses when the flux density is small ($\lambda = 1$). This occurred in the first time segment of the artificial random process: only two pulses fell in the first 10 s interval instead of anticipated ten on average. These two pulses are present in the upper plot of Figure 2. They are separated in time, so that their individual complex Fourier-transforms are correspondingly shifted in phase, and the relevant sum in the resulting spectrum acquires an interference pattern distorting the regular resonance outline. The greater is the inter-pulse delay, the more rapid are the interference oscillations. Since each of pulses additionally has an individual resonance outline depending on the particular source–observer distance, the distortions are the sinusoidal beating superimposed on a complicated spectral outline.

We illustrate in Figure 6 the power spectra of the first and the second 10 s segments of the synthesized time realization when $\lambda = 1$. One may observe that signal spectrum in the second time interval is characterized by the habitual irregular noise while the spectrum of the first time segment shows "sinusoidal beating". We also depict the original time realizations of the 10 s duration above individual spectra in Figure 6.

As we noted before, we cut the first 5 seconds of the synthetic record to avoid the transient process and the edge effects. Therefore, the first data segment ranges from 5 to 15 s "absolute" time, and the second one occupies the interval from 15 to 25 s.

The time domain plots explain the cause of regular beating in the power spectrum of the first time segment. Only two pulses are visible in this fragment of time realization shown in the inset of the upper plot of Figure 6. The onsets of both pulses are negative indicating the positive polarity of their parent lightning strokes. Amplitude of the second pulse substantially exceeds that of the first one. The inset of

the lower plot indicates that the second 10 s fragment of artificial time realization contains eleven pulses. Eight of them arrived from the negative (more probable) lightning strokes. A substantial number of pulses, their random amplitudes and delays cause very strong irregular fluctuations in the spectral density corresponding to the second temporal fragment of synthetic record.

Pulses in the time domain realizations of Figure 6 show a rapid decrease in time, and one may observe that a time interval $t_p = 0.3$ is quite sufficient for the correct accounting of a single radio pulse involved in the composition of artificial time record. Besides the fluctuating curves, we show the resonance curves in Figure 6 by the smooth lines, which were obtained from the particular power spectra with the singular spectrum analysis ["Caterpillar" algorithm, see Danilov and Zhiglyavsky, 1997 and Troyan and Hayakawa, 2002]. Such a processing also regarded as singular value decomposition extracts readily the hidden modes from the noisy spectra of elementary realizations. We will use the singular spectrum analysis below for separating the random fluctuations from the hidden regular spectral pattern. The "Caterpillar" procedure also allows us to evaluate the relative contribution of noise into the full energy of spectrum curve.

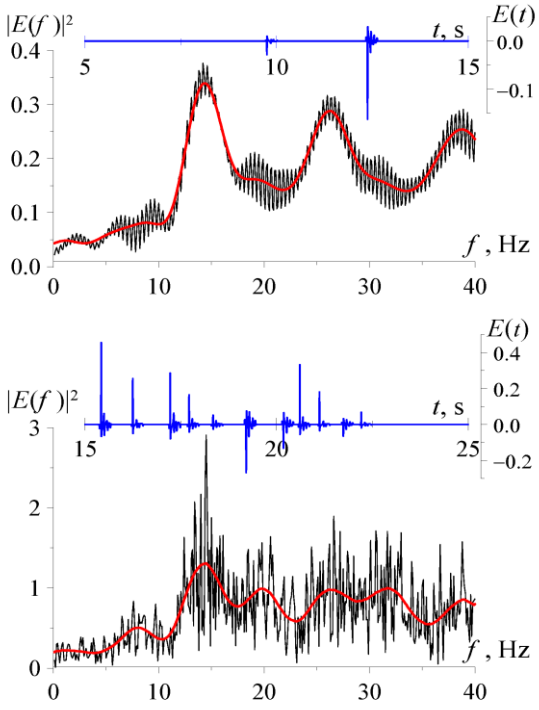

Figure 6: Spectra relevant to the first two 10 s fragments of realization for λ = 1.

8. Effect of flux density in the observed spectral outline

It is natural to suppose that the rate of spectral stabilization depends both on the accumulation time (the atmospherics flux density is constant) and on the flux density (the accumulation time is fixed). We will check this assumption below by using synthesized records of different flux densities.

Figure 7 contains two panels. The upper panel (Figure 7a) shows the model spectra computed with two completely different flux rates $\lambda = 1$ (the bottom pair) and $\lambda = 110$ events per second (the upper couple of curves). We depict spectra for accumulation time of 5 and 10 minutes here, and spectra corresponding to the smaller accumulation time are found below, together with the spectra accumulated during the longer time interval.

The computed spectra are shown in Figure 7a by thin black lines, and the thick red lines depict relevant spectral patterns deduced by the "Caterpillar" algorithm. We used three principal components found by "Caterpillar" procedure. Obviously, outline of all smoothed spectra is similar, and deviations relevant to flux rates of 1 and 110 pulses/s are comparable with those between the curves obtained for different accumulation times when the flux rate is fixed.

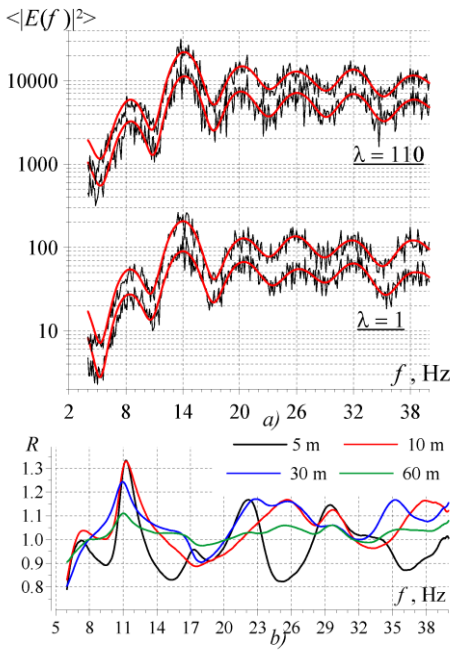

Figure 7: Comparison of the power spectra for different flux densities of atmospherics and duration of data accumulation.

The lower plots (Figure 7b) illustrate mutual deviations in the smoothed spectra against frequency. Here, the ordinate represents the ratio R of the smoothed spectral densities corresponding to flux λ = 1 and λ = 110 when the accumulation time is equal to 5, 10, 30, and 60 minutes. To construct these plots, we used the power spectra accumulated over the specified intervals, eliminated the fluctuations using the singular spectrum analysis, and computed the following ratio:

$$R(f) = 110\frac{S_1^T(f)}{S_{110}^T(f)}, \tag{6}$$

where $S^T_1(f)$ and $S^T_{110}(f)$ denote the smoothed power spectra obtained for the accumulation time T and the flux densities λ = 1 and λ = 110 shown by the sub-index.

We show plots obtained for the accumulation times of 5, 10, 30 and 60 minutes in Figure 7b. As might be seen, the relative deviations are approximately equal to ±20%, and the only exception is the case of T = 60 min, for which the maximum deviations do not exceed 10%. Thus, SR spectra obtained for the accumulation times of 5–10 minutes with the subsequent smoothing of spectral estimates by using the singular spectrum analysis are essentially independent of the particular flux density of lightning discharges, which form the natural electromagnetic noise in the ELF range. This property was always tacitly accepted in measurements. Now, we were able to demonstrate validity of this assumption by using the model time domain SR signal.

Data of Figure. 5 and 7 indicate that spectral stabilization is almost independent of the flux rate. This feature is of fundamental importance for implications of experimental SR data. Based on simulations performed here, we argue that the experimentally observed resonance parameters (peak frequencies and the quality factors) are governed rather by the global properties of the lower ionosphere and spatial distribution of the source–observer distances than by the pulse flux density. The non-averaged power spectra are not appropriate for the purpose, because they retain the noisy nature and strongly depend on the statistics of random sources.

9. Pulse rate that might be found from spectral stabilization

It is clear from intuitive considerations that stabilization rate of spectra should depend on the flux density of the arriving pulses. Of course, the actually observed flux density is high ranging from 50 to 100 pulses

per second, which is significantly higher than the 8 Hz fundamental frequency of SR. 6-12 random pulses arrive an observer during a single period of fundamental oscillation on average. The pulsed waveforms substantially overlap thus impeding inferring their amount. The model signal allows us to estimate the flux density giving a chance to assess the rate λ from the SR records.

Let us turn to dependence of the relative level of fluctuations in the power spectra on the accumulation time. We will use the conventional method of data processing in observations for the purpose. We construct the power spectra for the accumulation time of 5, 10 and 30 minutes and for the fixed flux densities λ = 1, 10, 50, 110 events per second. The resulting elementary spectra $S^5_\lambda(f)$, $S^{10}_\lambda(f)$, and $S^{30}_\lambda(f)$ are averaged over the one-hour observations, so that relevant ensembles contain 12, 6 and 2 spectra correspondingly. Thus we obtain the average spectra $G_5(f)$, $G_{10}(f)$, and $G_{30}(f)$. Afterwards, we compute the integral value Q of the relative square deviations in the frequency band of 4-40 Hz:

$$Q = \sum_{f_k=4}^{f_k=40} \frac{100}{G_T^2(f_k)} \left\{ \sum_N [S_T(f_k) - G_T(f_k)]^2 \right\} \tag{7}$$

Summation in the outer sum is performed over the frequencies varying from 4 to 40 Hz with a step of 0.1 Hz. Index T denotes the accumulation time, and the summation of the square deviations in the inner sum incorporates N terms: N = 12 when T = 5 min; N = 6 when T = 10min, and N = 2 when T = 30 minutes.

Obviously, the quantity Q depends on the accumulation time T and on the pulse flux rate λ, the latter playing the role of a parameter. The computed results are shown in Figure 8. Here, the horizontal axis depicts the accumulation time, and the vertical axis shows the relative fluctuations in the power spectra on logarithmic scale. Four curves are shown corresponding to 1, 10, 50, and 110 pulses per second. One may observe that magnitude of fluctuations considerably reduces when the accumulation time increases.

As was expected, all dependencies are very close when the flux density exceeds 10 pulses per second. Having in mind the stochastic nature of the model, we must accept these plots being coincident. The curve for the pulse rate of 1 stroke per second behaves similarly to all others, but it is elevated above the horizontal axis. This indicates that, in principle, the SR data allow estimating the number of the planetary lightning strokes, provided that their rate is small. The most delicate point here is the physical meaning of the term “small”.

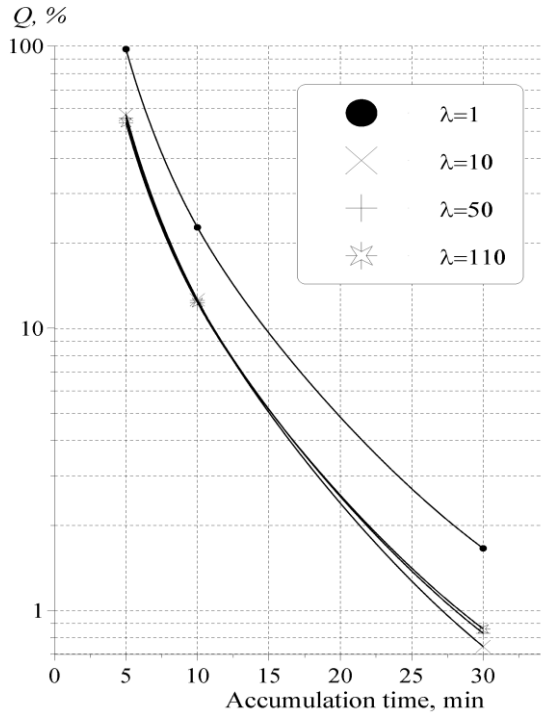

Figure 8: Relative spectral fluctuations against the accumulation time for different densities of atmospheric flux.

The criterion of small number in the unit time is the quantity of impulsive events found in the elementary realization used in the FFT algorithm, not the number of pulses in the fundamental period of resonance oscillations as might be expected. Obviously, this is a stronger criterion, and it is associated with the desire to have a profound spectral resolution. For terrestrial cavity with fundamental frequency of 8 Hz, the preferred spectral resolution is about 0.1 Hz. The corresponding duration equals to 10 s, which is the elementary time segment used in the FFT procedure. In order to make the spectral interference a function of pulse rate, this time interval should contain on average a few pulses only. Say, the flux density should be about 1 event per second. Under this condition, stability of spectral estimates significantly depends both on the accumulation (averaging) time and on the flux density-λ. Unfortunately, this possibility hardly might be implemented in the global electromagnetic resonance records preformed in the Earth–ionosphere cavity because the pulse flux is too high, in a range from 50 to 100 events per second.

10. Summary and conclusion

We described a way of generating the artificial time domain realization of ELF radio noise that simulates the actual SR records. The signal is a succession of random pulses each found from the solution of SR problem in the time domain. To obtain the model signal, one must use the random variables with the exponential, normal, and uniform distributions. The first of them is used in obtaining the mutual time delay of pulses; the second one describes the random amplitudes of lightning strokes; and the third one is used in creating an ensemble of random source–observer distances. We confined ourselves to the vertical electric field component, which allowed using of only three independent random variables. To simulate the horizontal magnetic field, one would have to add a random variable describing azimuth of the field source. In the simplest case, it might have a uniform distribution.

Application of pre-defined pseudo-random sequences has guaranteed the similarity and "reproduction" of signal properties when obtained with various values of the flux rate. In elaborating other model records of SR signal, one might imply the generation of random variables concurrently with computing the time realization of the field components.

Spectral processing was performed for the synthetic pulse sequences with rates of 1, 10, 50 and 110 events per second and for the time realization exceeding the 1-hour in duration. Using the standard 10-second segments of the records in the FFT procedure, we demonstrated that the artificial signal has many features of actual records. The major of them were: the noisy fine structure in the power spectra of the long realization, and the natural stabilization of the accumulated (averaged) power spectra. The synthesized radio signal allowed for estimating the rate of spectral stabilization, and it allowed us to demonstrate that the accumulated spectra are practically independent of the flux density of random atmospherics exceeding 10 pulses per second. Simulations showed that resonance pattern is determined by the properties of the Earth–ionosphere cavity. In other words, simulations confirm that the power spectra of SR background signal allow us to study the lower ionosphere.

Averaged spectra become rather smooth and have the maximum fluctuations of 20-30% when accumulation time reaches 5–10 minutes. These figures are consistent with observations of natural radio signals. A substantial accumulation time and weak dependence on the flux density λ arise from the Poisson nature of the random signal.

Spectral fluctuations do not disappear completely when the accumulation time increases. The relative fluctuations in the power spectra reduce to the level of 1–10% when the accumulation time reaches one hour, and they decrease vaguely with a further increase in accumulation time.

The flux density of arriving pulses might be evaluated from the records of the global electromagnetic resonance under certain conditions. The interval of flux rates in which the records of the global electromagnetic resonance become dependent on λ is governed by the desired spectral resolution. A few pulses from lightning strokes must fall on average within the elementary segment of the time domain realization used in the FFT procedure. For the terrestrial cavity, this condition results in the equality $\lambda \approx 1$ pulse per second, which is much smaller than the actual atmospheric flux rate from the global thunderstorms. Application of global electromagnetic resonance for assessing the atmospherics rate might be possible at planets smaller than Earth on the condition that there is a thunderstorm activity, and this activity is less intense than on the Earth.

The synthetic radio signal successfully models experimental records. It might be used as a reference record when testing and calibrating receiving equipment at remote observatories. Its application might become especially helpful for the data reduction to a standard format when acquired at different observatories.

References

Danilov D.L. and A.A. Zhiglyavsky , Principal Components of the Time Series: the Caterpillar Method, St.-Petersburg state University, St-Petersburg, Russia, pp. 307, 1997.

Myand S. V., A. P. Nickolaenko, L. M. Rabinowicz, I. G. Kudintseva, and M. Hayakawa, Time-domain representation of ELF pulses generated by lightning discharges, *Telecommunications and Radio Engineering*, **55**, No.4, pp. 1–8, 2001.

Nickolaenko A. P., One-dimensional distribution function of the vertical electric component of terrestrial ELF radio noise, *Radiophysics and Quantum Electronics*, **24**, No. 1, pp. 24-30, 1981.

Nickolaenko A. P., Natural ELF electromagnetic pulses, *Telecommunications and Radio Engineering*, **51**, No.1, pp. 25-34, 1997.

Nickolaenko A.P., and M. Hayakawa, Natural electromagnetic pulses in the ELF range, *Geophys. Res. Lett.*, **25**, No.16, pp. 3103-3106, 1998.

Nickolaenko A.P. and M. Hayakawa, Resonances in the Earth-Ionosphere Cavity, Kluwer Academic Publishers, Dordrecht, pp. 38, 2002.

Nickolaenko A. and M. Hayakawa, Schumann Resonance for Tyros (Essentials of Global Electromagnetic Resonance in the Earth–Ionosphere Cavity), Springer, Tokyo, PP. 348, 2014.

Nickolaenko A.P., and L.M. Rabinowicz, Acceleration of the convergence of time domain presentations for the ELF pulses from the lighting strokes, *Telecommunications and Radio Engineering*, **55**, No.5, pp. 16 – 22, 2001.

Nickolaenko A.P., L.M. Rabinowicz, and M. Hayakawa, Time domain presentation for ELF pulses with accelerated convergence, *Geophys. Res. Lett*., **31**, L05808, doi:10,1029/2003GL018700, 2004a.

Nickolaenko, A.P., L.M. Rabinowicz, and M. Hayakawa, Natural ELF pulses in the time domain: series with accelerated convergence, *IEEJ Trans. Fundamentals and Materials*, **124**, No.12, pp. 1210 – 1215, 2004b.

Schumann W.O., Über die strahlungslosen Eigenschwingungen einer leitenden Kugel, die von einer Luftschicht und einer Ionosphärenhülle umgeben ist, *Z. Naturfirsch*, **7a**, pp. 149–154, 1952.

Tikhonov V.I.,Statistical Radio Technique, Second Ed., Moscow, Radio and Communications, pp. 624 (in Russian), 1982.

Troyan V. N., and M. Hayakawa, Inverse Geophysical Problems, TERRAPUB, Tokyo, pp. 289, 2002.

